

Seasonal prediction of regional surface air temperature and first-flowering date over South Korea

Jina Hur and Joong-Bae Ahn*

Division of Earth Environmental System, Pusan National University, South Korea

ABSTRACT: The forecast capability of the first-flowering date (FFD) over South Korea is evaluated using the seasonal (1- to 3-month lead) prediction from the global [Pusan National University (PNU) coupled general circulation model (CGCM) v1.1] and regional [Weather Research and Forecast (WRF) v3.0] climate models. Gridded data with high spatial (3 km) and temporal (daily) resolution are produced using the physically based dynamical models. Dynamical downscaling is performed using WRF v3.0 with the lateral forcing from hourly outputs of PNU CGCM v1.1. Statistical correction is then used to eliminate systematic bias in the model output. The FFDs of cherry, peach and pear in South Korea are predicted for the decade of 1999–2008 by applying the corrected daily temperature predictions to the phenological thermal-time model. The WRF v3.0 results reflect the detailed topographical effect, despite having cold and warm biases for warm and cold seasons, respectively. After applying the correction, the mean temperature for early spring (February to April) clearly represents the general pattern of observation, while preserving the advantages of dynamical downscaling. The FFD predictabilities for the three species of trees are evaluated in terms of qualitative, quantitative and categorical estimations. Although FFDs derived from the corrected WRF results well predicted the spatial distribution and the variation of observation, the prediction performance has no statistical significance or appropriate predictability. Even though the upcoming flowering phenology could not be accurately predicted, the present study approach may be helpful in obtaining detailed and useful information about FFD and regional temperature by accounting for physically based atmospheric dynamics.

KEY WORDS seasonal prediction; regional temperature; cherry first-flowering date; pear first-flowering date; peach first-flowering date; dynamical downscaling

Received 14 June 2014; Revised 10 January 2015; Accepted 2 March 2015

1. Introduction

Flowering time closely affects tourism through festivals (Chung *et al.*, 2009, 2011) and agricultural productivity due to spring frost damage, pollination and fruit setting (Cannell and Smith, 1986; Guedon and Legave, 2008). Therefore, flowering date prediction is economically important for growers and relevant decision-makers because it can help risk management and decision making and thus maximize potential benefits (Schwartz *et al.*, 1997).

Phenological models have been developed to predict flowering date by accounting for the thermal-time concept since the time of Réaumur (1735) (Linkosalo *et al.*, 2006). Substantial research (e.g. Chung *et al.*, 2009; Hur and Ahn, 2014; Hur *et al.*, 2014) has demonstrated that phenological models based on high-temperature requirement can successfully predict flowering time in deciduous tree species. Thus, reliable temperature prediction can facilitate skillful forecasting of flowering date.

Much of the effort in developing the general circulation model (GCM) has been devoted to providing long-term

weather and climate information with sufficient accuracy. However, despite the successful development of GCM over the last several decades, it remains incapable of obtaining station-based or high-resolution data due to its coarse-resolution grid system (Ahn *et al.*, 2012; Kang *et al.*, 2014). Thus, dynamical downscaling based on a regional climate model (RCM) has been used in conjunction with GCM, thereby offering long-term gridded data with high resolution.

Although a few studies (e.g. Chung *et al.*, 2009; Avolio *et al.*, 2012) have projected gridded temperature and flowering phenology using both GCM and dynamical downscaling, most of these focused on the future change of flowering phenology in association with global warming. Although the prediction of upcoming flowering phenology is essential and useful in many respects, insufficient research has been conducted on seasonal prediction in flowering date.

The objective of this study is to explore the prediction possibility of flowering date by applying seasonal temperature prediction with high resolution to the phenological thermal-time model. The two specific study aims are: (1) to obtain seasonal (1- to 3-month lead) temperature hindcasts on a daily basis with fine-scale grid spacing (3 km) using both GCM and dynamical downscaling over South Korea and (2) to predict the first-flowering dates (FFD) of three

* Correspondence to: J.-B. Ahn, Department of Atmospheric Sciences, Pusan National University, Busan, South Korea.
E-mail: jbahn@pusan.ac.kr

deciduous trees (cherry, peach and pear) in South Korea during 1999–2008 by applying daily temperature hindcasts to the phenological model on a thermal-time basis.

2. Data and methods

2.1. Seasonal temperature prediction

In order to obtain the long-term temperature prediction with high-resolution grid spacing in South Korea, dynamical downscaling is performed using the Weather Research and Forecast (WRF) Model v3.0 developed by the National Center for Atmospheric Research (NCAR) (Skamarock *et al.*, 2008). The initial and boundary conditions for WRF are derived from hourly output of the Pusan National University coupled GCM (PNU CGCM) v1.1, a participant model of the Asia-Pacific Economic Cooperation (APEC) Climate Center (APCC) multi-model ensemble (MME) prediction system (Sun and Ahn, 2011, 2014).

2.1.1. Global climate model (PNU CGCM v1.1)

The global climate model used for long-range prediction is PNU CGCM v1.1, a fully coupled ocean–atmosphere–land–sea–ice model. The model consists of the 18-level National Center for Atmospheric Research Community Climate Model (CCM3, T42), the 29-level Geophysical Fluid Dynamics Laboratory Modular Ocean Model (MOM3), and the Los Alamos National Laboratory elastic viscous plastic sea-ice model (Sun and Ahn, 2011). Atmospheric and land variables have a horizontal resolution of 2.8125° , whereas oceanic variables have a variable grid in latitude with finer resolution at the equatorial region, i.e. 0.7° at lower latitudes below 30° , 1.4° at mid-latitude between 30° – 60° and 2.8° at higher latitudes above 60° . The model is described in more detail by Sun and Ahn (2011, 2014). PNU CGCM v1.1 is adopted because it is used by the APCC MME long-range prediction system and has already been used successfully in the earlier studies (e.g. Sun and Ahn, 2011, 2014; Kim and Ahn, 2012; Ahn and Kim, 2014; Kang *et al.*, 2014), as a forcing for RCM.

Hourly outputs of PNU CGCM v1.1 are used for the decade from 1999 to 2008. The initial and boundary conditions of WRF v3.0 for this decade are made using atmospheric and land variables from PNU CGCM v1.1 such as vertical and horizontal wind components, temperatures, relative humidities, soil moistures and soil temperatures.

2.1.2. Regional climate model (WRF v3.0)

Dynamical downscaling is performed using WRF v3.0 RCM with the lateral forcing from hourly outputs of PNU CGCM v1.1. RCM is a fully compressible non-hydrostatic model with an Arakawa-C grid system (Hong and Lee, 2009). The model configuration consists of two-way interactive triple-nested domains with 3 km-, 9 km- and 27 km-resolution centering on South Korea. A two-way nesting is used in the study by considering its better performance compared to one-way option, which allows

for interactions between outer and inner domains (Moeng *et al.*, 2007; Harris and Durran, 2010). Each domain has 28 vertical levels from the surface up to 50 hPa. A 3-day spin-up period is adopted by considering the time required for the dynamical adjustment between lateral forcing and the internal physical dynamics of the model (Ahn *et al.*, 2012). For the model physics schemes, we selected WRF Single-Moment 6-class (Hong and Lim, 2006), Kain–Fritsch (Kain and Fritsch, 1993) and Yonsei-University (Hong and Dudhia, 2004) for microphysics, cumulus and planetary boundary processes, respectively. More detailed configuration for WRF v3.0 is presented in Ahn *et al.* (2012), although their system is for reproduction rather than prediction.

The integrations span the decade corresponding to the period of the lateral forcing's existence. The analysis is only focused on the daily surface air temperature with 3-km grid spacing derived from the third inner domain over South Korea (124.34° – 130.30° E, 33.845° – 38.652° N).

2.1.3. Bias correction

Although the prediction system is well constructed using the refined climate models, the model cannot predict accurately due to many uncertainties from initial and boundary conditions, the model physics and parameterizations. The application of a statistical correction technique to the model results can help to reduce these problems. In this study, the simple statistical correction method is adopted to minimize the systematic biases in the RCM output.

Systematic bias is defined as the mean state difference between the prediction and observation. Therefore, only the mean state of the model is corrected under its anomaly preservation (Ahn *et al.*, 2012). Our correction method is comprised of the following three steps. In the first step, we divide the prediction $P(k, t)$ and the observation $O(k, t)$ at grid point k and in time t into the mean part ($\overline{P(k)}$, $\overline{O(k)}$) and the perturbation (anomaly) part ($P(k, t)'$, $O(k, t)'$) using the perturbation method.

$$P(k, t) = \overline{P(k)} + P(k, t)', \quad (1)$$

$$O(k, t) = \overline{O(k)} + O(k, t)'. \quad (2)$$

In the second step, the difference (Bias(k)) in the mean parts between prediction and observation is calculated and termed a bias. The bias is estimated using leave-one-out cross-validation.

$$\text{Bias}(k) = \overline{P(k)} - \overline{O(k)} \quad (3)$$

Then, the bias at each grid point is area-averaged within the diameter, 12.7 km, which is the mean distance of the observation stations, to eliminate the noise induced by the interpolation.

$$\text{Bias}_{\text{mave}}(k) = \sum_{n=1}^{Rn} \text{Bias}(n) / Rn, \quad (4)$$

where Rn is the number of grid points within the diameter (12.7 km) at the center, grid point k .

Table 1. Three parameters for the DTS model that are determined to be the most suitable values by root mean square errors (RMSE) analysis.

	Cherry	Peach	Pear
<i>Ds</i> (JD)	37	34	44
<i>Ea</i> (KJ mol ⁻¹)	60	72	64
<i>DTS</i> (days)	122.1	162.7	145.8

In the third step, finally, the statistically corrected prediction (*Pc(k, t)*) is produced by subtracting the area-averaged bias (*Bias_{mave}(k)*).

$$Pc(k, t) = (\overline{P(k)} - Bias_{mave}(k)) + P(k, t) \quad (5)$$

Hereafter, the prediction without correction will be referred to as U_WRF, and the corrected prediction as C_WRF.

2.2. Flowering date prediction

The FFDs of three deciduous trees (cherry, peach and pear) in South Korea are predicted using the number of days transformed to standard temperature (DTS) model, which is a kind of thermal-time phenological model (Ono and Konno, 1999). The DTS model is selected in this study because of its good performance in estimating the three FFDs in South Korea (Hur and Ahn, 2014; Hur *et al.*, 2014). Mathematically, DTS is based on the sum of the exponential function of the daily average temperature (Hur and Ahn, 2014).

$$\sum_{t=1}^{nday} (daily\ DTS)_{tk} = \sum_{t=1}^{nday} (\exp(Ea(T_{tk} - T_s) / R \cdot T_{tk} \cdot T_s)) \quad (6)$$

where *T_{tk}* is the daily average surface air temperature, and daily *DTS_{tk}* is the daily DTS accumulation at the grid point *k* on the *tth* day since the starting day of calculation (*Ds*). *T_s*, *R* and *Ea* indicate the standard temperature (271.4 K), the universal gas constant (8.314 J K⁻¹ mol⁻¹) and the sensitivity of plants to temperature, respectively. For the DTS model, the three parameters are optimized for each species of trees: (1) *Ds* (Julian Day, JD); (2) *Ea*, the temperature sensitivity rate (KJmol⁻¹); and (3) *DTS*, the accumulated daily DTS from *Ds* to FFD (days) (Ono and Konno, 1999; Aono and Kazui, 2008; Aono and Saito, 2010; Hur and Ahn, 2014; Hur *et al.*, 2014). As in Hur and Ahn (2014), the FFDs are estimated with 120 combinations [12 (the number of *Ds*) × 10 (the number of *Ea*)], and then the best combination with the lowest root mean square error (RMSE) between the observed and estimated FFDs is determined (Table 1). This approach enables different parameters to be obtained according to the kind of tree. More detailed explanation on the parameterization is presented in Hur and Ahn (2014).

After construction of the phenological model, the daily temperature predicted by the climate model is applied to the DTS model. Then, the predictability of FFD is evaluated by comparison with *in situ* observation.

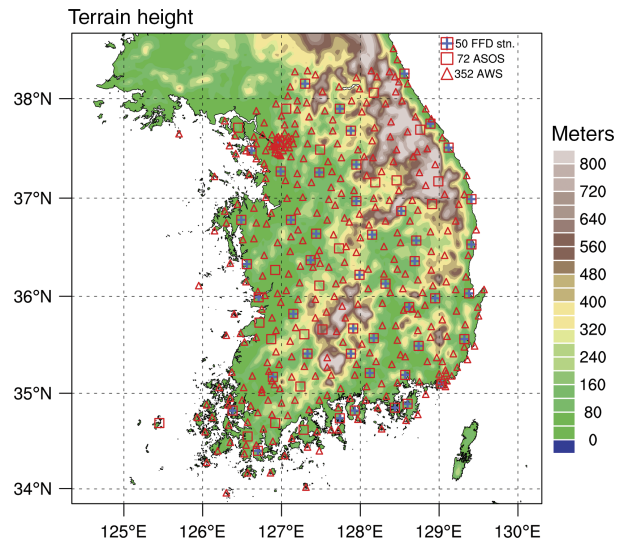


Figure 1. Locations of 72 ASOS (red squares) and 352 AWS (red triangles) for temperature and 50 stations (red squares with blue cross) observing the FFDs of cherry, peach and pear in South Korea.

2.3. Meteorological and phenological observation data

The daily average surface air temperatures observed at 72 automated surface observation systems (ASOS) and 352 automatic weather stations (AWS) for the decade of 1999–2008 are obtained from the Korean Meteorological Administration (KMA) to evaluate the temperature predictability and to estimate systematic bias in the model. To investigate the accuracy of the FFD prediction, the FFD observations from 50 observation sites over the same study period for cherry, peach and pear are used. The day of FFD is defined as when more than 20% of each tree’s buds are in full bloom. Figure 1 shows the location of the 72 ASOS and 352 AWS for surface air temperature and 50 stations for FFDs.

For comparison with the gridded temperature prediction, *in situ* observations are interpolated into the grid system (3 km) of the third-inner domain of RCM. For interpolation, Cressman objective analysis (Cressman, 1959) is used by setting the effective radii as 15 and 30 km for ASOS and 6 and 12 km for ASOS + AWS. These radii are selected by considering the average distance between the observation sites. Hereafter, ASOS, AWS and ASOS + AWS interpolated onto the C_WRF grid system (3 km) will be referred to as gridded ASOS, gridded AWS and gridded ASOS + AWS, respectively.

3. Results and discussions

3.1. Predictability of the daily surface air temperature

Several studies have already investigated the relationship between surface air temperature and the FFDs of these three species of trees in South Korea (Jeong *et al.*, 2011; Hur and Ahn, 2014). They found a strong correlation between the temperature of early spring [3 months from February to April (FMA)] and the three FFDs in South

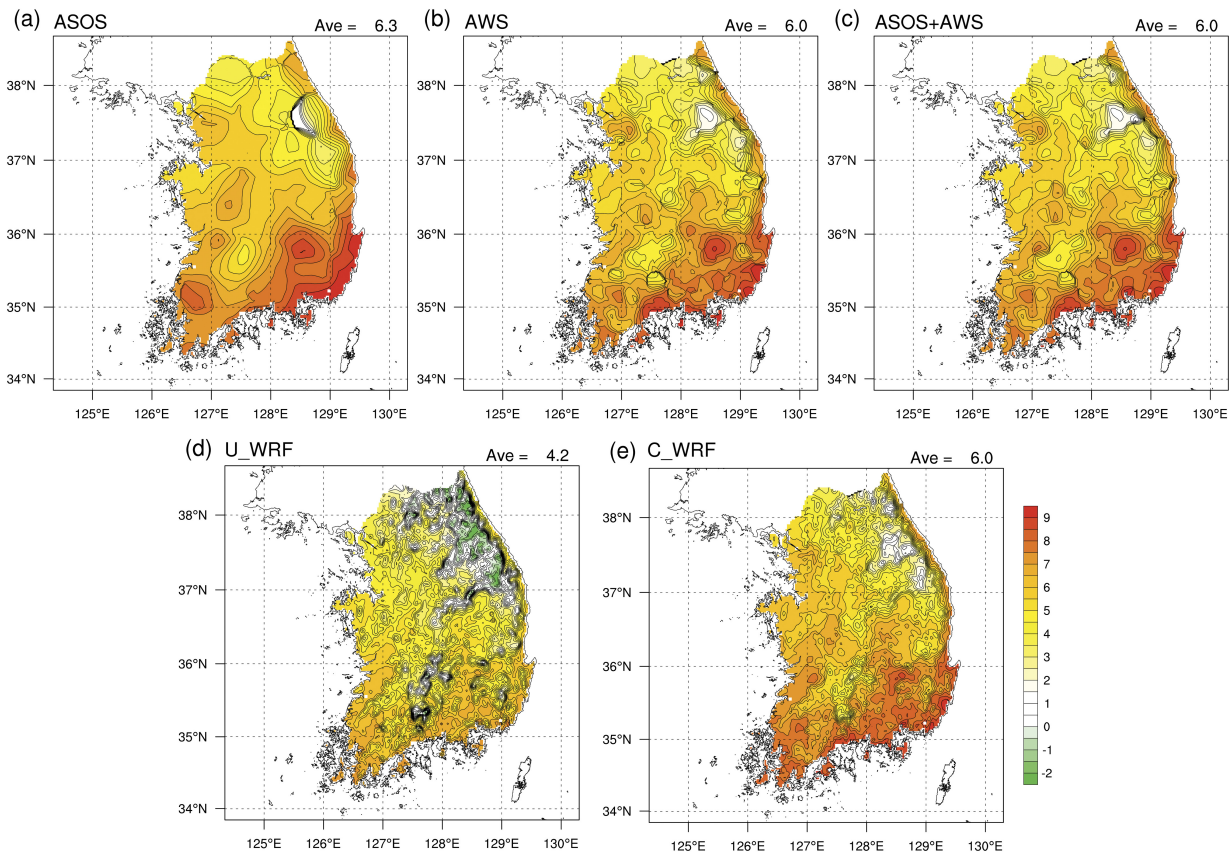


Figure 2. Distribution of surface air temperature over South Korea for early spring (FMA) averaged over the decade (1999–2008) derived from (a) ASOS, (b) AWS, (c) ASOS + AWS, (d) U_WRF and (e) C_WRF.

Korea. Therefore, this article investigates the predictability of early spring temperature.

First, the spatial distribution of surface air temperature for early spring (FMA) is investigated. Figure 2 shows the spatial distribution of the temperature averaged over the decade (1999–2008) derived from the gridded ASOS, the gridded AWS, the gridded ASOS + AWS, U_WRF and C_WRF for early spring. The temperature derived from ASOS on average is 6.3°C , which reflects the topographic effect roughly. The temperature in AWS and ASOS + AWS is 6.0°C , which follows the general spatial patterns and characteristics of ASOS. By comparison with ASOS, however, AWS and ASOS + AWS reflect a physiographical feature in more detail because of the greater number of AWS (352) compared to that of ASOS (72). In other words, the greater number of station sites reduces the average distance between observation sites, thereby increasing the precision of the distribution. Although the network in South Korea is sufficiently dense, the average distance of 12.7 km between ASOS + AWS sites remains insufficient to represent the detailed geographical features of South Korea, especially in the northeastern region due to its variant topography and fewer sites.

On the contrary, U_WRF with a grid spacing of 3 km generates a more detailed temperature distribution throughout South Korea, including the northeastern region. However, U_WRF underestimates the temperature for early spring due to a systematic bias. Qualitatively,

the temperature distribution of C_WRF reveals a greater similarity to the observation pattern than that of U_WRF, while maintaining the detailed topographical effect of RCM. That is, the systematic biases in the RCM results are significantly reduced by statistical correction, thereby affording more accurate prediction results. Quantitatively, the mean temperature of 4.2°C in U_WRF is increased to 6.0°C after statistical correction in C_WRF. That is, the trend toward underestimation in RCM output has been corrected, so that the prediction approaches closer to the observation (6.0°C in ASOS + AWS). The pattern correlation coefficient between C_WRF and ASOS + AWS is also increased by about 0.14–0.93 in comparison with U_WRF (0.79).

The daily variabilities of observation and prediction are analyzed. Figure 3 displays the time series of daily mean temperatures averaged over the decade derived from ASOS, ASOS + AWS, U_WRF and C_WRF. Here, for the comparison with observation, U_WRF and C_WRF are interpolated onto *in situ* ASOS + AWS sites. In ASOS and ASOS + AWS, the highest and lowest temperatures appear in the summer (JJA) and winter (DJF) seasons, respectively. Overall, U_WRF shows some discrepancies with observation due to systematic biases, despite its good prediction of the general temporal pattern of observation. As in the case of Ahn *et al.* (2012), temperature was underestimated in the warm season and overestimated in the cold season. In C_WRF, the general fluctuation of

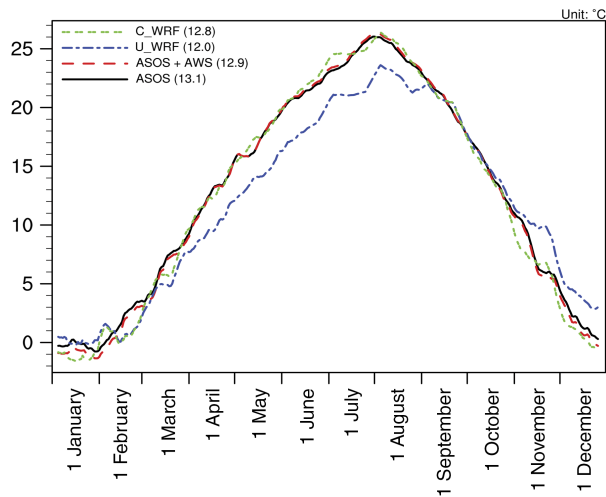


Figure 3. Daily mean temperature averaged over the decade (1999–2008) derived from ASOS (black solid line), ASOS + AWS (red dash line), U_WRF (blue dash-dot line) and C_WRF (green dot-dot line) interpolated onto the 424 station sites in South Korea. The 10-day moving average is applied.

observation value is well captured, as is the daily mean temperature, by correcting the cold and warm biases of U_WRF. The annual mean temperature of C_WRF is 12.8 °C, which is 0.8 °C higher than the 12.0 °C of U_WRF and 0.1 °C lower than the 12.9 °C of ASOS + AWS, which is the value closest to observation. It is interesting to note the relatively large discrepancy between C_WRF and observation in February and March. It is probably because the correction method used in the study can be applied only to the mean field of model outputs and the daily fluctuation during the period is relatively large as compared to the other months. Thus, in spite that the monthly mean field of C_WRF is in good agreement with observation, daily variations of the temperature are not well produced due to the larger fluctuation in U_WRF for the period. The prediction skill of FFDs may be somewhat mediated by the discrepancy.

We investigated the characteristics and predictabilities of surface air temperature in mountainous complex terrain by focusing on the northeast region (Gangwon-do) of South Korea. Figure 4 displays the spatial distribution of surface air temperature (shaded) derived from gridded ASOS, gridded ASOS + AWS and C_WRF over Gangwon-do for early spring. To examine the influence of topography on temperature, topography (contoured) and station sites were overlaid on the temperature distribution. In ASOS and ASOS + AWS, the temperatures are higher at low altitude and in flatlands than at high altitude. However, low temperature does not clearly appear along the mountain ridges. Observation stations, especially ASOS, are located in low-lying areas for ease of maintenance and power supply (Ahn *et al.*, 2012). Therefore, the map derived solely from ASOS distorts the realistic temperature distribution in mountainous areas. Although gridded ASOS + AWS considers more stations than ASOS, it remains insufficient to represent the temperature characteristics on the mountain

ridges. In comparison, C_WRF effectively expresses both the detailed topographical effect and the overall pattern of gridded ASOS + AWS.

The altitude dependency of surface air temperature is also investigated using the temperature field in Figure 4. We focus on the Gangwon-do region as in the case of Ahn *et al.* (2012) in order to avoid latitudinal temperature differences and focus on the temperature change with altitude. Figure 5 presents scatterplots of altitudes against temperature over the mountainous area of Gangwon-do. The temperatures averaged over the decade are derived from in-situ OBS (ASOS + AWS), gridded OBS (ASOS + AWS) and C_WRF over Gangwon-do. In Figure 5, temperatures observed at 77 sites are used for *in situ* OBS, whereas those at 4408 grid points are used for gridded OBS and C_WRF over Gangwon-do. Temperature is strongly dependent on altitude in the *in situ* OBS. The surface air temperatures in gridded OBS and C_WRF also decrease with increasing altitude. Gridded OBS and C_WRF have the advantage of gaining information on a series of temperatures at altitude higher than 900 m. However, the distribution of gridded OBS presents a widely scattered pattern with a dull edge, because the interpolation method (Cressman method) only considers the distance and most of the observation stations are in lower sites. On the contrary, the distribution of C_WRF is well organized as a function of altitude with a rather sharp edge, which indicates that the topographical effect is properly reflected in C_WRF. Therefore, climate models in conjunction with statistical correction method can properly predict the altitude dependency of temperature appearing in observation by reflecting the detailed topographic effect.

3.2. Predictability of the FFD

In the previous section, we investigated the accuracy of the temperature prediction produced by climate models and bias correction. In this section, we evaluated the predictability of FFDs using the daily temperature prediction validated in the previous section. Although we investigated the analysis results for the three species of trees of cherry, peach and pear, we present these results simultaneously to avoid duplication.

First, the temporal change in accumulated DTS is explored. Figure 6 shows the change of accumulated DTS derived from observation and C_WRF, in associated with daily temperature (see Section 2.2). For the comparison, C_WRF is interpolated onto the 50 FFD observation sites in South Korea. The daily DTS is accumulated from each Ds until the DTS requirement (DTS in Table 1) is satisfied for each species of trees. If $\sum \text{daily DTS} \geq \text{DTS}$, FFD occurs and the accumulation of daily DTS stops. In observation, the DTS accumulation grows linearly until early- or mid-April. Overall, C_WRF clearly predicts the variation of observation despite some discrepancy; i.e. the floral development is reasonably predicted on a daily basis.

Prior to the quantitative analysis, qualitative analysis is performed by investigating the distribution of the three

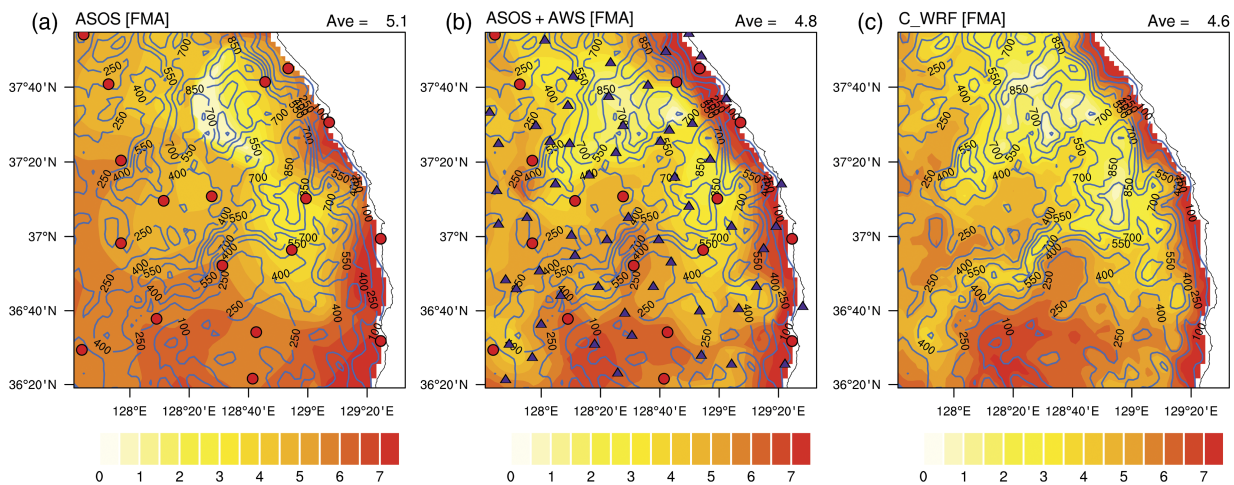


Figure 4. Topography (contoured, m) and distribution of surface air temperature (shaded, °C) over the Gangwon-do mountainous region in South Korea for early spring (FMA) averaged over the decade (1999–2008) derived from (a) ASOS, (b) ASOS + AWS and (c) C_WRF. Red dot and blue triangle denote the locations of ASOS and AWS sites, respectively.

FFDs in South Korea. Figures 7–9 show the spatial distributions for the 10-year (1999–2008) averaged FFDs derived from *in situ* observation, gridded observation and C_WRF for cherry, peach and pear, respectively. The average FFDs observed at *in situ* stations are JD 93.2, 96.8 and 100.3 for cherry, peach and pear, respectively, i.e. the trees flower in the order of cherry, peach and pear, on average. In the *in situ* observation, the station sites located in low latitude and flat areas have relatively earlier FFD than those in high latitude and mountainous regions due to their low temperatures. This spatial structure of observation appears for all three species of trees. There is no remarkable difference in the spatial distribution among the three species of trees. The gridded observation maintains the general characteristics of *in situ* observation with the average of JD 94.8, 98.4 and 101.7 for cherry, peach and pear, respectively. However, the gridded observation distribution shows very coarse values and cannot express landforms properly because of the paucity of stations in the mountain regions. C_WRF expresses the topographical effect in detail, while maintaining the overall observation pattern. C_WRF has an average of JD 98.4, 101.7 and 105.5 for cherry, peach and pear, respectively, in South Korea. Thus, cherry is predicted to flower about 3.3 and 7.1 days faster than peach and pear, respectively, which are similar values with those in *in situ* and gridded observations. It is also interesting to note that average FFDs observed at the *in situ* stations are about 1.5 and 5 days faster than those derived from the gridded observation and C_WRF, respectively. It can be attributed to the discrepancy in mean altitude between the *in situ* observation site and the model's grid point. In detail, the third inner domain of WRF has an average height of 215.3 m, which is three times higher than the mean altitude of the observation sites (74.7 m).

The distribution of FFDs according to altitude is also examined. Figure 10 displays the scatterplots of the altitude of 50 stations against FFDs derived from the *in situ* observation and C_WRF. For comparison with

in situ observation, C_WRF is interpolated onto the 50 *in situ* observation sites in South Korea. The regression lines for observation and C_WRF are illustrated in Figure 10. In the observation, FFD is delayed with increasing elevation of the observation site. The FFD delay rate with elevation is 4.3, 4.9 and 3.9 days/100 m for cherry, peach and pear, respectively. Peach shows the regression line with the steepest slope, followed in order by cherry and pear. It indicates that peach has more sensitivity to altitude than cherry and pear. The altitude dependency of FFD shown in the observation also appears in C_WRF. However, FFDs derived from C_WRF are generally earlier than those of observation at high elevation. This is attributed to the temperature lapse rate in observation being steeper than that in C_WRF (see Figure 5). The FFD discrepancies between the observation and C_WRF at high altitude are relatively larger in peach than those in the other two trees. In other words, C_WRF better simulated the altitude dependency of FFD in cherry and pear cases.

Finally, the FFD performance is evaluated based on both quantitative and categorical estimations such as temporal correlation coefficient (TCC), RMSE and hit rate (HR). Prior to evaluation, C_WRF is interpolated onto the 50 *in situ* observation sites in South Korea for comparison. Hence, all calculations are performed at each station, and then averaged over 50 FFD stations. Categorical estimation (i.e. HR) is performed using three categories based on $0.53 \times$ standard deviation (σ) for each species of trees: below normal ($< -0.53 \sigma$), normal ($\geq -0.53 \sigma$ and $\leq 0.53 \sigma$) and above normal ($> +0.53 \sigma$). The three categories (below normal, normal above normal) indicate that approximately 30, 40 and 30% of the total events occur, respectively. Table 2 shows the average, standard deviation and the skill scores of the three FFDs. Average FFDs derived from C_WRF are similar to those of the observation within a narrow margin of 2 days. The standard deviations of predicted FFDs range from 3.48 to 3.87 days, whereas those of observations are more

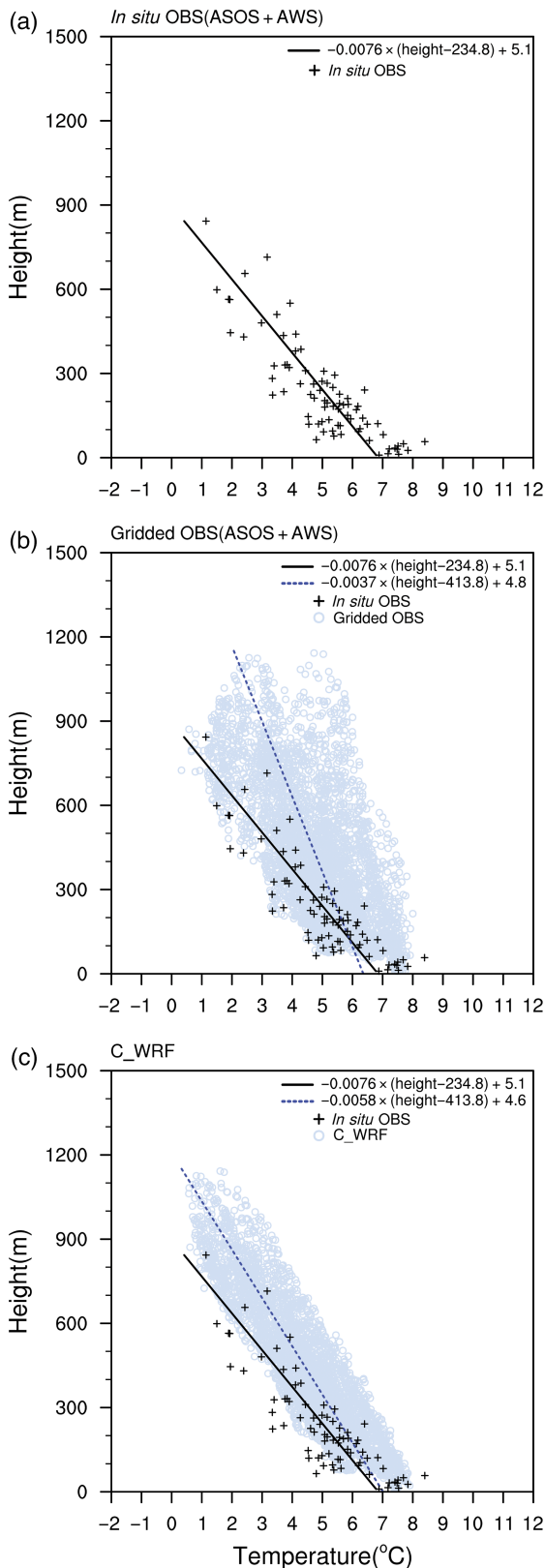


Figure 5. Scatterplots of altitude against temperature and its regression line (blue dashed line) over the Gangwon-do mountainous region in South Korea for early spring (FMA), averaged over the decade (1999–2008) derived from (a) *in situ* ASOS + AWS, (b) gridded ASOS + AWS interpolated onto C_WRF grid system and (c) C_WRF. Here, the distributions of *in situ* ASOS + AWS (black cross) and its regression line (black solid line) are illustrated in all panels for reference.

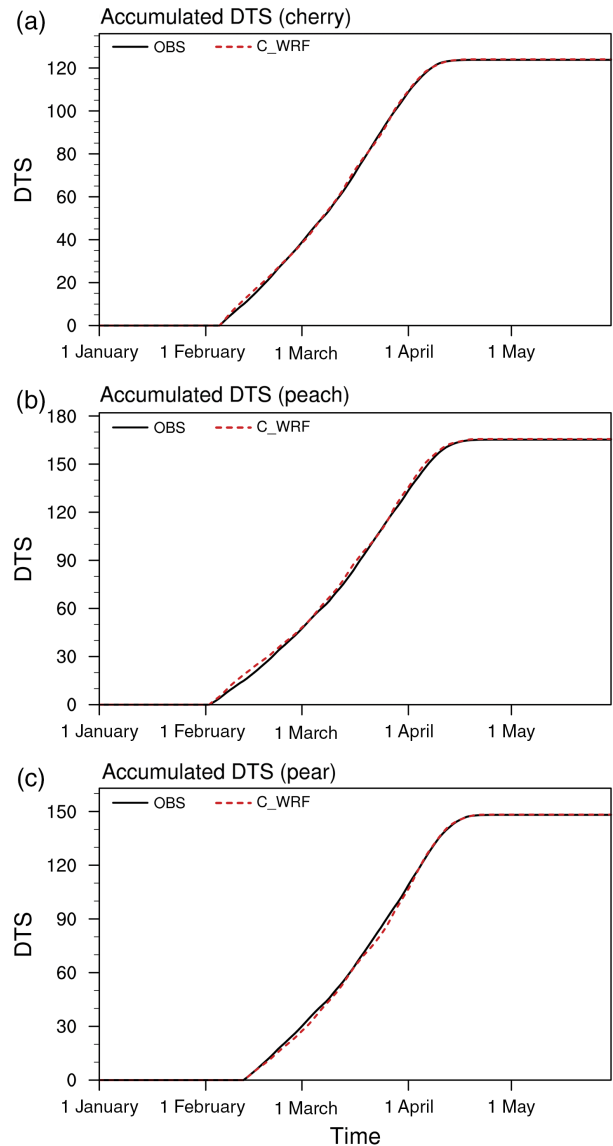


Figure 6. Accumulated DTS change over time for cherry, peach and pear trees. The data are averaged over the decade (1999–2008) derived from the 50 FFD stations (black solid line) and C_WRF (red dashed line) interpolated onto the 50 station sites in South Korea.

than 4.1 days, implying that the DTS model systematically underestimates the temporal variations of FFDs. In terms of RMSE, C_WRF can predict FFDs for the three species of trees with a discrepancy of about 5 days with observation. TCC ranged from 0.29 to 0.36, which is not statistically significant. HR is about 0.40 (+0.05% as a range), i.e. 40% of the cases are correctly predicted by the model. Although FFDs are well predicted using the combination of C_WRF and DTS model from the qualitative standpoint, this methodology has limited performance in terms of quantitative and categorical evaluations.

To further investigate this limitation of FFD predictability, an additional experiment is conducted using observed temperature. First, FFDs are newly estimated by applying observed temperature to DTS phenological model. Then, their performances are evaluated as in the case of Table 2. Table 3 shows the skill of the DTS phenological model

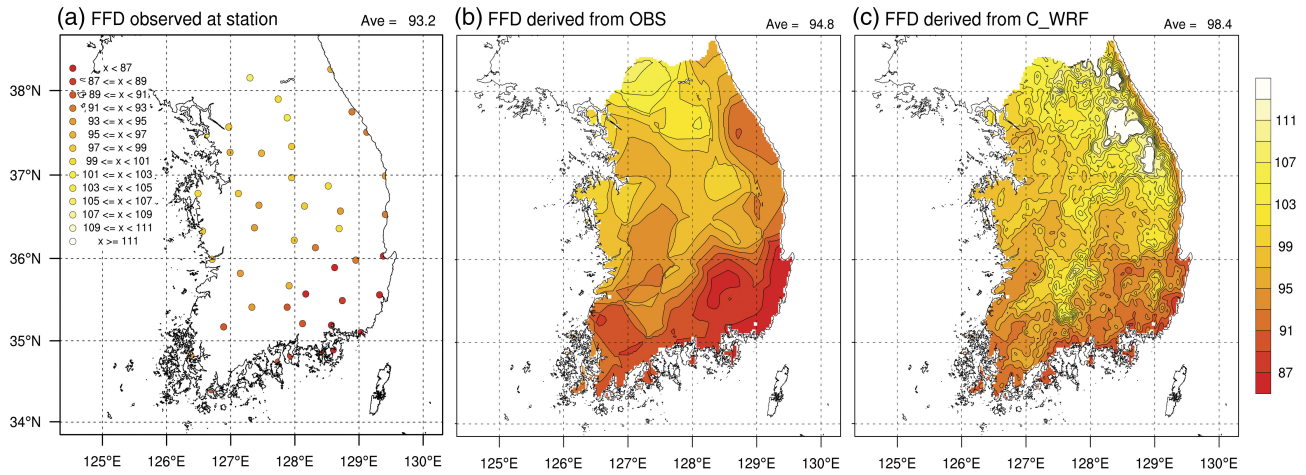


Figure 7. Spatial distribution of cherry FFD derived from (a) *in situ* observation, (b) gridded observation and (c) C_WRF averaged for the decade (1999–2008). Unit is Julian day.

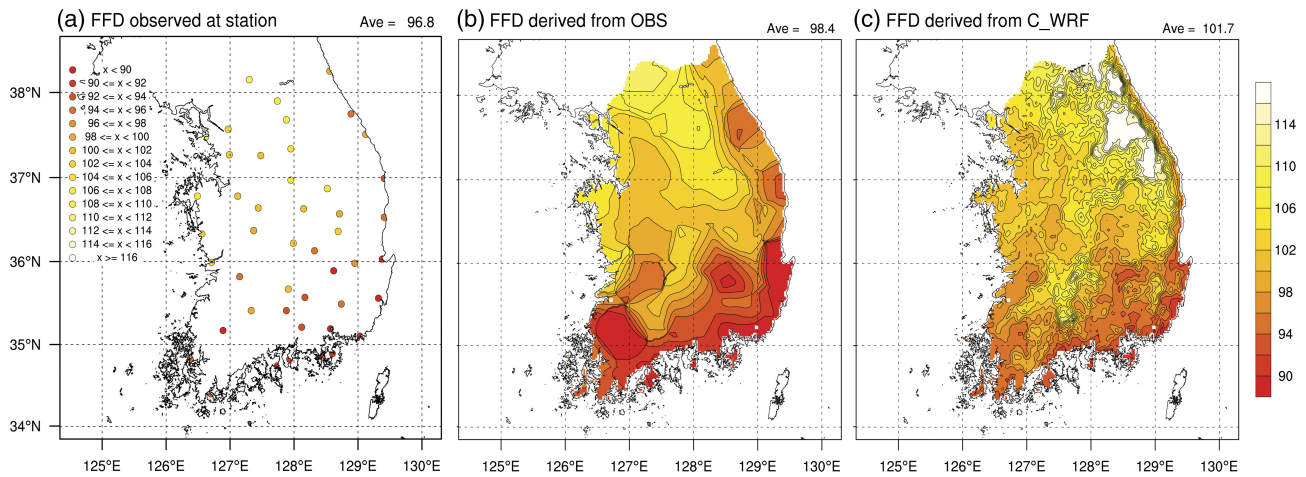


Figure 8. Spatial distribution of peach FFD (a) *in situ* observation, (b) gridded observation and (c) C_WRF averaged for the decade (1999–2008). Unit is Julian day.

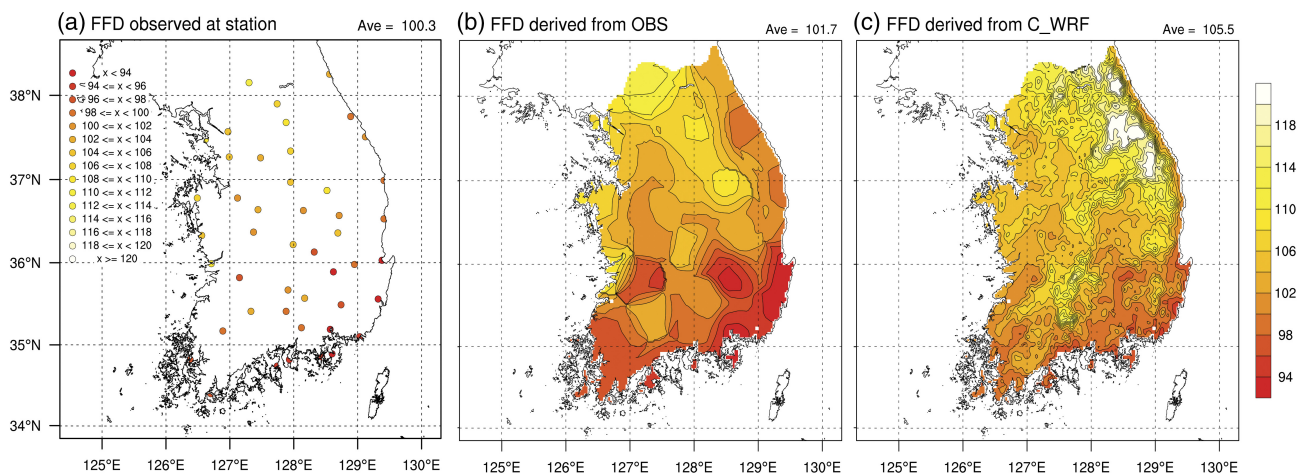


Figure 9. Spatial distribution of pear FFD (a) *in situ* observation, (b) gridded observation and (c) C_WRF averaged for the decade (1999–2008). Unit is Julian day.

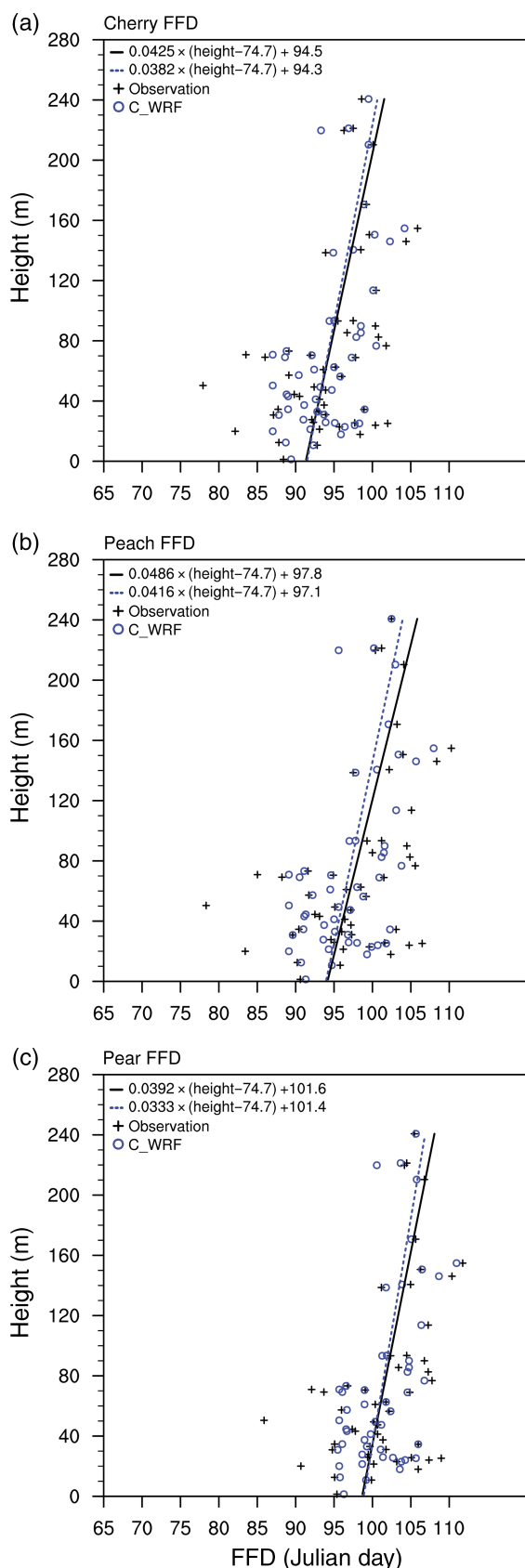


Figure 10. Scatterplots of the altitude of 50 stations against (a) cherry, (b) peach and (c) pear first-flowering date (FFD) derived from the observation (black cross) and C_WRF (blue circle) interpolated onto the *in situ* observation sites in South Korea. The black solid and blue dashed lines denote regression lines for the observation and C_WRF, respectively.

by assuming that the observed temperature is perfect input data. In Table 3, the RMSEs are lower than 3.35 days, indicating that the DTS model can estimate the FFDs of cherry, peach and pear in South Korea with a difference of about 3 days from observation. The TCCs are 0.82, 0.74 and 0.73 for cherry, peach and pear, respectively, which is statistically significant at the 95% confidence level. The DTS model also exhibits good performance in terms of categorical estimation. Although the DTS phenological model has the lower temporal variations, it can provide FFD information with high accuracy under the condition of perfect input data. Therefore, the limitation of FFD predictability can be attributed mainly to the low temperature accuracy, i.e. imperfect input data, rather the phenological thermal-time model. In other words, the limitation of C_WRF seems to reduce the predictability of the FFDs for cherry, peach and pear in South Korea.

4. Conclusion and summary

In this study, the capability of forecasting FFD over South Korea is evaluated using the seasonal (1- to 3-month lead) prediction with high-resolution grid spacing (3 km) on a daily basis. For the study, global-scale gridded meteorological variables for the decade of 1999–2008 are produced using the PNU CGCM v1.1 seasonal prediction system on an hourly basis. Then, dynamical downscaling is performed using WRF v3.0 RCM with lateral forcing from the hourly outputs of PNU CGCM v1.1. The RCM outputs are statistically corrected to reduce systematic biases, thereby affording reliable prediction of surface air temperature. The FFDs of cherry, peach and pear in South Korea are predicted for the decade of 1999–2008 by applying these daily temperatures to the DTS phenological model.

The results from RCM (U_WRF) clearly reflect the detailed topographical effect. However, due to systematic biases, the temperature prediction is underestimated during early spring. After correction is applied, the mean temperature for early spring equates to that (6.0°C) of the observation, while maintaining the advantage of dynamical downscaling. Overall, the corrected prediction (C_WRF) clearly represents the general pattern of observation as well as landform. Therefore, reliable and detailed information on daily temperature can be obtained using climate models and the statistical correction method.

The predictability of FFD is evaluated for each species of trees using various estimations. Qualitatively, FFDs derived from C_WRF well predict the spatial distribution and its variation in the observation. However, in quantitative and categorical estimations, the prediction performance has no statistical significance or great predictability. In an additional experiment, we find that the limitation of FFD predictability can be mainly attributed to the low accuracy of the input data. In other words, C_WRF cannot predict the FFDs with great accuracy, even though the climate model well simulates the general characteristics

Table 2. Average (Ave), standard deviation (Std) and skill scores of FFD prediction interpolated onto the 50 *in situ* observation station sites.

	Prediction Ave/Observation Ave (JD)	Prediction Std/observation Std (Day)	Root mean square error (Day)	Temporal correlation coefficient	Hit rate
Cherry	94.32/93.18	3.87/4.14	4.15	0.36	0.43
Peach	97.05/96.76	4.16/4.81	5.34	0.29	0.40
Pear	101.37/100.28	3.48/4.62	4.61	0.30	0.45

*95% confidence level (± 0.63)

Table 3. Average (Ave), standard deviation (Std) and skill scores of FFD derived from temperatures observed at the 50 stations.

	Estimation Ave/Observation Ave (JD)	Estimation Std/observation Std (Day)	Root mean square error (Day)	Temporal correlation coefficient	Hit rate
Cherry	94.48/93.18	2.99/4.14	2.67	0.82*	0.72
Peach	97.77/96.76	3.34/4.81	3.35	0.74*	0.64
Pear	101.60/100.28	2.76/4.62	3.28	0.73*	0.64

*95% confidence level (± 0.63)

in observation. To increase the reliability of seasonal prediction, both climate and phenological models need to be improved.

The methodology used in the study can be applied to other locations. The DTS phenological model has already been used for analysis by some researchers and received favorable evaluations. This methodology, therefore, offers the advantage of being applicable to various locations and plants. Even though the upcoming flowering phenology could not be accurately predicted, the proposed approach may be helpful in obtaining detailed and useful information about FFD and regional temperature. Despite the importance of seasonal prediction, few studies have been performed to predict FFD by taking into account physically based atmospheric dynamics. Therefore, we believe that this approach will help in generating physically based gridded data for various plants over diverse regions with high spatial (less than 3 km) and temporal (less than daily) resolutions.

Acknowledgements

This work was carried out with the support of the Rural Development Administration Cooperative Research Program for Agriculture Science and Technology Development under Grant Project No. PJ009353, Republic of Korea.

References

- Ahn J-B, Kim HJ. 2014. Improvement of 1-month lead predictability of the wintertime AO using a realistically varying solar constant for a CGCM. *Meteorol. Appl.* **21**: 415–418, doi: 10.1002/met.1372.
- Ahn J-B, Lee J, Im E-S. 2012. The reproducibility of surface air temperature over South Korea using dynamical downscaling and statistical correction. *J. Meteorol. Soc. Jpn.* **90**: 493–507, doi: 10.2151/jmsj.2012-404.
- Aono Y, Kazui K. 2008. Phenological data series of cherry tree flowering in Kyoto, Japan, and its application to reconstruction of springtime

- temperatures since the 9th century. *Int. J. Climatol.* **28**: 905–914, doi: 10.1002/joc.1594.
- Aono Y, Saito S. 2010. Clarifying springtime temperature reconstructions of the medieval period by gap-filling the cherry blossom phenological data series at Kyoto, Japan. *Int. J. Biometeorol.* **54**: 211–219, doi: 10.1007/s00484-009-0272-x.
- Avolio E, Orlandi F, Bellecci C, Fornaciari M, Federico S. 2012. Assessment of the impact of climate change on the olive flowering in Calabria (southern Italy). *Theor. Appl. Climatol.* **107**: 531–540, doi: 10.1007/s00704-011-0500-2.
- Cannell MGR, Smith RI. 1986. Climatic warming, spring budburst and frost damage on trees. *J. Appl. Ecol.* **23**: 177–191.
- Chung U, Jung J-E, Seo H-C, Yun JI. 2009. Using urban effect corrected temperature data and a tree phenology model to project geographical shift of cherry flowering date in South Korea. *Clim. Change* **93**: 447–463, doi: 10.1007/s10584-008-9504-z.
- Chung U, Mack L, Yun JI, Kim S-H. 2011. Predicting the timing of cherry blossoms in Washington, DC and mid-Atlantic states in response to climate change. *PLoS One* **6**(11): e27439, doi: 10.1371/journal.pone.0027439.
- Cressman GP. 1959. An operational objective analysis system. *Mon. Weather Rev.* **87**: 367–374.
- Guedon Y, Legave JM. 2008. Analyzing the time-course variation of apple and pear tree dates of flowering stages in the global warming context. *Ecol. Model.* **219**: 189–199, doi: 10.1016/j.ecolmodel.2008.08.010.
- Harris LM, Durran DR. 2010. An idealized comparison of one-way and two-way grid nesting. *Mon. Weather Rev.* **138**: 2174–2187, doi: 10.1175/2010MWR3080.1.
- Hong S-Y, Dudhia J. 2004. Testing of a new non-local boundary layer vertical diffusion scheme in numerical weather prediction applications. In *20th Conference on Weather Analysis and Forecasting/16th Conference on Numerical Weather Prediction*, Seattle, WA, Presentation/webcast, 14 January 2004.
- Hong S-Y, Lee J-W. 2009. Assessment of the WRF model in reproducing a flash-flood heavy rainfall event over Korea. *Atmos. Res.* **93**: 818–831, doi: 10.1016/j.atmosres.2009.03.015.
- Hong S-Y, Lim J-OJ. 2006. The WRF single-moment 6-class microphysics scheme (WSM6). *J. Korean Meteorol. Soc.* **42**(2): 129–151.
- Hur J, Ahn J-B. 2014. The change of first-flowering date over South Korea projected from downscaled IPCC AR5 simulation: peach and pear. *Int. J. Climatol.*, doi: 10.1002/joc.4098.
- Hur J, Ahn J-B, Shim K-M. 2014. The change of cherry first-flowering date over South Korea projected from downscaled IPCC AR5 simulation. *Int. J. Climatol.* **34**: 2308–2319, doi: 10.1002/joc.3839.
- Jeong J-H, Ho C-H, Linderholm HW, Jeong S-J, Chen D, Choi Y-S. 2011. Impact of urban warming on earlier spring flowering in Korea. *Int. J. Climatol.* **31**: 1488–1497, doi: 10.1002/joc.2178.

- Kain JS, Fritsch JM. 1993. Convective parameterization for mesoscale models: the Kain-Fritsch scheme. In *The Representation of Cumulus Convection in Numerical Models*. Meteorological Monographs No. 24. American Meteorological Society: Boston, MA, 165–170.
- Kang S, Hur J, Ahn J-B. 2014. Statistical downscaling methods based on APCC multi-model ensemble for seasonal prediction over South Korea. *Int. J. Climatol.* **34**: 3801–3810, doi: 10.1002/joc.3952.
- Kim HJ, Ahn J-B. 2012. Possible impact of the autumnal North Pacific SST and November AO on the East Asian winter temperature. *J. Geophys. Res.* **117**: D12104, doi: 10.1029/2012JD017527.
- Linkosalo T, Hakkinen R, Hanninen H. 2006. Models of the spring phenology of boreal and temperate trees: is there something missing? *Tree Physiol.* **26**: 1165–1172.
- Moeng C-H, Dudhia J, Klemp J, Sullivan P. 2007. Examining two-way grid nesting for large eddy simulation of the PBL using the WRF model. *Mon. Weather Rev.* **135**: 2295–2311, doi: 10.1175/MWR3406.1.
- Ono S, Konno T. 1999. Estimation of flowering date and temperature characteristics of fruit trees by DTS method. *Jpn. Agric. Res. Q.* **33**: 105–108.
- Réaumur RAF. 1735. Observations du thermomètre, faites à Paris pendant l'année 1735, comparées avec celles qui ont été faites sous la ligne, à l'Isle de France, à Alger et en quelquesunes de nos isles de l'Amérique. *Mém. Acad. R. Sci.* **1735**: 545–576.
- Schwartz MD, Reighard GL, Okie WR. 1997. A model to predict peach phenology and maturity using meteorological variables. *HortScience* **32**: 213–216.
- Skamarock WC, Klemp JB, Dudhia J, Gill D, Barker D, Dudhia M, Huang XY, Wang W, Powers JG. 2008. A description of the advanced research WRF Version 3. NCAR Technical Note No. NCAR/TN-475+STR, NCAR, Boulder, CO, 113 pp.
- Sun J, Ahn J-B. 2011. A GCM-based forecasting model for the landfall of tropical cyclones in China. *Adv. Atmos. Sci.* **28**: 1049–1055, doi: 10.1007/s00376-011-0122-8.
- Sun J, Ahn J-B. 2014. Dynamical seasonal predictability of the arctic oscillation using a CGCM. *Int. J. Climatol.*, doi: 10.1002/joc.4060.